

A diRNA–protein scaffold module mediates SMC5/6 recruitment in plant DNA repair

Jieming Jiang ¹, Xiaolin Ou ¹, Danlu Han ¹, Zhipeng He ¹, Song Liu ¹, Ning Mao ¹,
Zhonghui Zhang ¹, Chang-Lian Peng ¹, Jianbin Lai ^{1,*} and Chengwei Yang ^{1,*}

¹ Guangdong Provincial Key Laboratory of Biotechnology for Plant Development, School of Life Science, South China Normal University, Guangzhou 510631, China

*Authors for correspondence: yangchw@scnu.edu.cn (C.Y.); 20141062@m.scnu.edu.cn (J.L.)

C.Y. and J.L. designed experiments and supervised the research. J.J. and X.O. conducted experiments. D.H., Z.H., S.L., N.M., Z.Z., and C.L.P. provided technological supports. J.J., J.L., and C.Y. analyzed data and wrote the manuscript.

The author responsible for distribution of materials integral to the findings presented in this article in accordance with the policy described in the Instructions for Authors (<https://academic.oup.com/plcell>) is Chengwei Yang (yangchw@scnu.edu.cn).

Abstract

In eukaryotes, the STRUCTURAL MAINTENANCE OF CHROMOSOME 5/6 (SMC5/6) complex is critical to maintaining chromosomal structures around double-strand breaks (DSBs) in DNA damage repair. However, the recruitment mechanism of this conserved complex at DSBs remains unclear. In this study, using *Arabidopsis thaliana* as a model, we found that SMC5/6 localization at DSBs is dependent on the protein scaffold containing INVOLVED IN DE NOVO 2 (IDN2), CELL DIVISION CYCLE 5 (CDC5), and ALTERATION/DEFICIENCY IN ACTIVATION 2B (ADA2b), whose recruitment is further mediated by DNA-damage-induced RNAs (diRNAs) generated from DNA regions around DSBs. The physical interactions of protein components including SMC5–ADA2b, ADA2b–CDC5, and CDC5–IDN2 result in formation of the protein scaffold. Further analysis indicated that the DSB localization of IDN2 requires its RNA-binding activity and ARGONAUTE 2 (AGO2), indicating a role for the AGO2–diRNA complex in this process. Given that most of the components in the scaffold are conserved, the mechanism presented here, which connects SMC5/6 recruitment and small RNAs, will improve our understanding of DNA repair mechanisms in eukaryotes.

Introduction

DNA damage is induced by a variety of endogenous and exogenous factors during the development of all organisms (Friedberg et al., 2004). DNA double-strand breaks (DSBs), one of the most serious forms of DNA damage, severely reduce genomic stability and cell viability, and even result in cancers in animals (Jackson and Bartek, 2009; Schubert, 2021). Several strategies including cell cycle control, programmed cell death, and DNA repair have evolved to respond to DSBs (Su, 2006; Hu et al., 2016). Non-homologous end joining (NHEJ) and homologous recombination (HR) are two primary pathways for DSB repair (Puchta, 2005;

Ceccaldi et al., 2016). The NHEJ pathway utilizes a simple repair mechanism via directly rejoining DSBs (Lieber, 2010). Unlike NHEJ, which ultimately generates genomic mutations, HR relies on homologous sequences and precise recruitment of repair factors to improve repair accuracy (Kowalczykowski, 2015).

The DNA damage response (DDR) facilitates the recruitment of a series of DNA repair factors to DNA break sites and the production of single-strand DNA (ssDNA) tails for subsequent repair (Waterman et al., 2020). First, ATAXIA-TELANGIECTASIA MUTATED (ATM) or ATM/RAD3-RELATED (ATR) is activated for phosphorylation of H2A.X

around DSBs (Gobbini et al., 2013; Turinetto and Giachino, 2015). Studies have shown that phosphorylated H2A.X promotes acetylation of histone H3 and recruitment of the chromatin remodeling SWITCH/SUCROSE NONFERMENTABLE (SWI/SNF) complex in mammalian cells, which in turn enhances the exposure of DNA damage sites via chromatin remodeling (Lee et al., 2010). The ends of the DSB sites are then recognized and cleaved by the complex containing MEIOTIC RECOMBINATION 11, RADIATION SENSITIVE (RAD) 50, and NIJMEGEN BREAKAGE SYNDROME 1, to produce ssDNA tails (Syed and Tainer, 2018), and are subsequently bound by the heterotrimeric protein complex REPLICATION PROTEIN A (RPA) for the synthesis of DNA damage-induced RNA (diRNA) (Wei et al., 2012; Liu et al., 2017; Storici and Tichon, 2017). Conserved among eukaryotes, ARGONAUTE 2 (AGO2) is a predominant effector protein associated with diRNAs (Wei et al., 2012; Gao et al., 2014). Under the guidance of the diRNA-AGO2 complex, a dsRNA-binding protein INVOLVED IN DE NOVO 2 (IDN2) is recruited to DSBs and interacts with RPA to promote its release from ssDNA tails and enhance the recruitment of RAD51 for subsequent HR in plant cells (Liu et al., 2017).

STRUCTURAL MAINTENANCE OF CHROMOSOME (SMC) complexes, including cohesin (SMC1/3), condensin (SMC2/4), and the SMC5/6 complex, have important roles during DNA repair (Jeppsson et al., 2014; Yatskevich et al., 2019). The SMC5/6 complex primarily contributes to chromosome structure maintenance in HR and is conserved among eukaryotic species (Murray and Carr, 2008; Aragón, 2018). For instance, depletion of the components of SMC5/6 has been shown to result in HR defects in yeast, plant, and human cells (Harvey et al., 2004; Potts et al., 2006; Watanabe et al., 2009). A critical question is how the SMC5/6 complex is precisely recruited at DSBs; however, the factors regulating this process vary among different organisms. The BREAST CANCER SUSCEPTIBILITY GENE1 Carboxyl-Terminal domain-containing protein REGULATOR OF TY1 TRANSPOSITION 107 (RTT107) was first identified in the DSB localization of SMC5/6 in *Saccharomyces cerevisiae* (Leung et al., 2011). In mammals, the SMC5/6 complex interacts with the SMC5-SMC6 COMPLEX LOCALIZATION FACTOR PROTEIN 1/2 (SLF1/SLF2) dimer, which links to RAD18 near DNA damage sites (Räschle et al., 2015). In *Arabidopsis thaliana*, a transcriptional co-activator ALTERATION/DEFICIENCY IN ACTIVATION 2B (ADA2b) interacts with SMC5 for recruitment of the SMC5/6 complex to DSBs (Lai et al., 2018; Jiang et al., 2019). However, the original factor by which the above-mentioned protein scaffolds are determined for DSB recruitment of SMC5/6 remains unclear in all species.

In this study, we found that CELL DIVISION CYCLE 5 (CDC5), a subunit of the MOS4-ASSOCIATED COMPLEX (MAC) complex associated with RNA splicing and miRNAs biogenesis (Lin et al., 2007; Zhang et al., 2013), is an adaptor that connects ADA2b and IDN2. Thus, diRNAs generated by

DNA damage mediate the precise localization of the IDN2-CDC5-ADA2b scaffolds for recruitment of the SMC5/6 complex at DSBs in plant cells. This study provides evidence of a functional association between small RNAs and SMC5/6 recruitment and improves our understanding of general DNA repair mechanisms.

Results

CDC5 interacts with ADA2b and participates in DNA repair

Precise localization of the SMC5/6 complex at DSBs is essential for its function in DNA repair in eukaryotic cells (Díaz and Pecinka, 2018). Our previous study showed that ADA2b, a co-transcriptional activator, mediates the DSB recruitment of SMC5/6 (Lai et al., 2018); however, the factors that determine the correct localization of ADA2b at DSBs remained completely unknown. Therefore, we performed a yeast two-hybrid assay to identify the ADA2b-interacting partner using a small library of chromatin-associated proteins including HEAT SHOCK TRANSCRIPTION FACTOR A2, SWITCH/SUCROSE NONFERMENTING 3A, MYC2, CDC5, MAC3a, IDN2, HISTONE DEACETYLASE (HDA)6, HDA19, ASYMMETRIC LEAVES 2, and BRAHMA. In this assay, only CDC5 was found to interact with ADA2b in yeast cells (Figure 1A). Further detailed analysis indicated that the N-terminal regions of CDC5 and ADA2b were their interacting domains (Supplemental Figure S1). The physical interaction between CDC5 and ADA2b was confirmed using an in vitro pull-down assay, in which ADA2b-FLAG was precipitated specifically with the MBP-tagged CDC5 (Figure 1B). The data from the in vivo precipitation assay indicated that ADA2b bound to CDC5 in plant cells (Figure 1C).

CDC5 is a subunit of the MAC complex involved in microRNA biogenesis and RNA splicing in plants (Zhang et al., 2013). If the association between CDC5 and ADA2b is essential for SMC5/6 recruitment, CDC5 may also be essential for DNA damage repair. To test this hypothesis, we compared the phenotypes of *CDC5* and *ADA2b* mutant plants. Reverse transcription-quantitative real-time polymerase chain reaction (RT-qPCR) data showed that depletion of either *CDC5* or *ADA2b* resulted in a significant increase in transcripts of DDR genes (Figure 1D). Moreover, the results of a comet assay indicated that DNA damage accumulated in both the *CDC5* and *ADA2b* mutant plants (Figure 1, E and F) and the percentages of accumulated DNA in tails were restored in the complementary plants (Supplemental Figure S2, A and B). Then propidium iodide (PI) staining was used to detect cell death in root meristems, which is possibly associated with DNA damage. Cell death was observed in the root meristems of the *CDC5* mutant seedlings, even without DNA-damaging treatments. Under treatment with methyl methanesulfonate (MMS), a DNA-damage reagent, the areas of cell death in the root meristems of the *CDC5* and *ADA2b* mutants were significantly larger than those in wild-type plants (Figure 1, G and H). The MMS sensitivity of the root meristem was also restored to wild-type

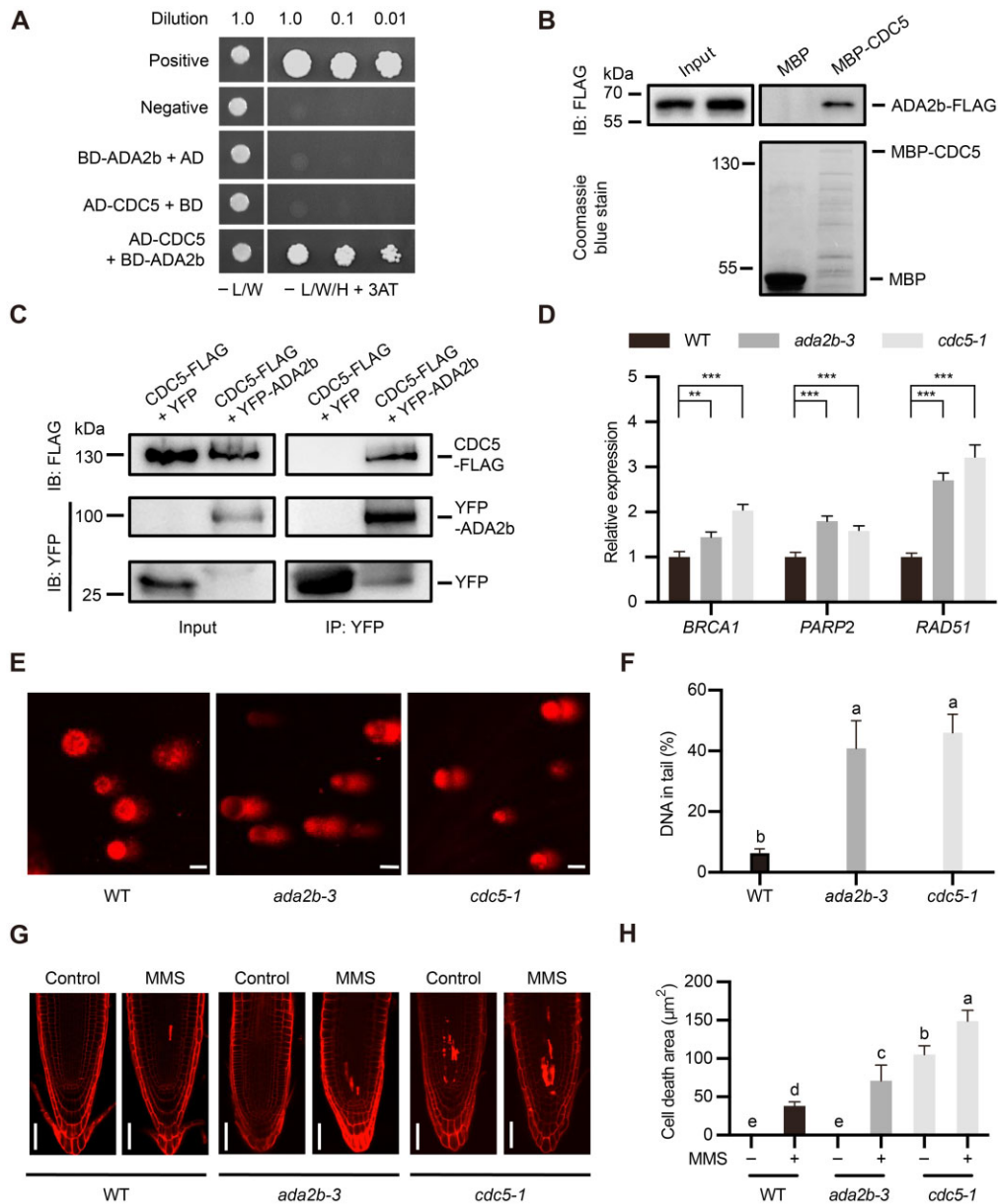


Figure 1 CDC5 interacts with ADA2b and participates in DNA repair. **A**, The interaction between CDC5 and ADA2b was detected by yeast two-hybrid assay. ADA2b was fused with binding domain (BD) and CDC5 was fused with activation domain (AD); the interaction was tested on SD/-Leu/-Trp/-His medium containing 5-mM 3-AT. **B**, The interaction between CDC5 and ADA2b was measured by in vitro pull-down assay. MBP-tagged CDC5 or free MBP (negative control) was used for precipitation of ADA2b-FLAG. Levels of MBP and MBP-CDC5 were measured by Coomassie blue staining, and ADA2b-FLAG was detected using an anti-FLAG antibody. **C**, In vivo interaction of ADA2b and CDC5 was detected by co-immunoprecipitation assay. CDC5-FLAG was co-expressed with YFP-ADA2b or free YFP (negative control), and total protein was extracted for incubation with anti-GFP agarose. The lysates (left) and immunoprecipitated proteins (right) were detected using anti-GFP and anti-FLAG antibodies. **D**, The transcript levels of DDR genes were measured via RT-qPCR in 2-week-old ADA2b and CDC5 mutant plants. Data are mean \pm SD from four technical replicates using the same samples. *** $P < 0.001$, ** $P < 0.01$, Student's *t* test (two-tailed). Results are representative of three independent experiments (independent plant growth and sample preparation). **E** and **F**, Detection of genomic integrity in 3-week-old ADA2b and CDC5 mutant plants via comet assay. Representative images from three biologically independent experiments (independent plant growth and sample preparation) are shown in (**E**); bars, 25 μm . Percentages of DNA in the tail (mean \pm SD; $n = 15$) are shown in (**F**). Significant differences are indicated with different letters above the columns; $P < 0.001$, one way ANOVA followed by Tukey's multiple comparisons test. **G** and **H**, MMS sensitivity of ADA2b and CDC5 mutant plants. Five-day-old seedlings were transferred onto medium with or without 75- $\mu\text{g mL}^{-1}$ MMS, and images of root meristems with PI staining were obtained 2 days after transfer. Representative images from three biologically independent experiments (independent plant growth and treatment) are shown in (**G**); bars, 50 μm . Cell death areas were calculated using ImageJ; the data in (**H**) are mean \pm SD from 15 roots. Significant differences are indicated with different letters above the columns; $P < 0.001$, one way ANOVA followed by Tukey's multiple comparisons test.

levels in the *ADA2b* and *CDC5* complementary lines (Supplemental Figure S2, C and D). To exclude the possibility that the cell death was specifically caused by MMS, we tested the sensitivity of the *ADA2b* and *CDC5* mutants to Zeocin, a radiomimetic agent (Chankova et al., 2007). Both mutants were more sensitive to Zeocin than the corresponding wild-type plants, with lower survival rates (Supplemental Figure S3, A and B) and larger areas of cell death in the root meristems (Supplemental Figure S3, C and D). These phenotype analyses supported the notion that *CDC5* and *ADA2b* may work together in DNA repair in plant cells.

Recruitment of *ADA2b* at DSBs is mediated by *CDC5*

DNA damage induces phosphorylation of H2A.X at DSBs (Kinner et al., 2008). We have previously shown that both *ADA2b* and *SMC5* form foci that are co-localized with phosphorylated H2A.X at DSBs under MMS treatment (Lai et al., 2018; Jiang et al., 2019). Having shown that *CDC5* interacts with *ADA2b* and participates in DNA repair, the next question was whether *CDC5* was also localized at DSBs. Therefore, *CDC5* was fused with YFP and co-expressed with CFP-*ADA2b* or *SMC5*-CFP in protoplasts. Microscopy results showed that *CDC5* formed foci in the nucleus, which were co-localized with both *ADA2b* and *SMC5* under treatment with MMS (Supplemental Figure S4), supporting the DSB localization of *CDC5*.

To elucidate the recruitment mechanism of the partners of *CDC5*–*ADA2b* at DSBs, several experiments were performed to detect whether the foci formation by *ADA2b* and *CDC5* was mutually dependent. First, YFP-*CDC5* was expressed in wild-type and *ada2b-3* protoplasts with or without MMS treatment. YFP-*CDC5* was evenly distributed in the nucleus in both cell types under the normal condition (Figure 2, A and B). Under MMS treatment, YFP-*CDC5* was concentrated in nuclear foci in the majority of cells of both types (Figure 2, A and B), suggesting that the localization of *CDC5* at DSBs is independent of *ADA2b*. Similarly, YFP-*ADA2b* was expressed in the wild-type or *cdc5-1* cells for localization analysis. YFP-*ADA2b* was also found to be generally localized in the nucleus in both types of cells under the normal condition (Figure 2, C and D). When the cells were treated with MMS, YFP-*ADA2b* formed nuclear foci in the majority of wild-type cells but only in a very small proportion of *cdc5-1* cells (Figure 2, C and D), suggesting that the localization of *ADA2b* at DSBs is predominantly mediated by *CDC5*. Further analysis indicated that the foci formation of *SMC5*-YFP was also dependent on *CDC5* (Supplemental Figure S5), consistent with our previous conclusion that the DSB recruitment of *SMC5/6* was mediated by *ADA2b* (Lai et al., 2018).

To verify our conclusion in intact plants, genes encoding *ADA2b* or *CDC5* protein fused with YFP were introduced into the *ada2b-3* and *cdc5-1* mutants under a native promoter. The fertility of these mutants was restored, suggesting

that these YFP-fused proteins were functional. Both *ADA2b* and *CDC5* were localized in the nucleus and formed foci in the roots of complementary plants under MMS treatment (Figure 2E; Supplemental Figure S6). The foci formation of YFP-*CDC5* was not affected in the *ada2b-3* mutant roots (Supplemental Figure S6), but YFP-*ADA2b* was unable to form foci in the *cdc5-1* mutant roots (Figure 2E), supporting our conclusion from the protoplast experiments that *CDC5* mediates the DSB localization of *ADA2b*.

We observed that the recruitment of *ADA2b* at DSBs was impaired in the absence of *CDC5* during DNA damage; thus, an excess amount of *ADA2b* protein may improve its accumulation at DSBs and contribute to DNA repair. Therefore, we overexpressed *ADA2b* in *cdc5-1* mutant plants. Cell death in the meristem of *cdc5-1* roots was partially attenuated under both the normal (Supplemental Figure S7) and MMS treatment (Figure 2, F and G) conditions. Endogenous DNA damage was evaluated in 3-week-old plants in a comet assay; overexpression of *ADA2b* significantly restored the genomic integrity of the *cdc5-1* mutant plants (Figure 2, H and I), providing evidence of a functional association between *ADA2b* and *CDC5* during DNA repair.

IDN2 interacts with *CDC5* and participates in DNA repair

Having shown that *CDC5* is essential for the DSB localization of *ADA2b*, the next question was what factors determine the specific localization of *CDC5* at DSBs. Previous studies showed that diRNAs, which are small RNAs generated from DSBs, are important in DNA repair (Wei et al., 2012; Liu et al., 2017). Given that *CDC5* is involved in RNA splicing and small RNA processing (Zhang et al., 2013), it is possible that *CDC5* interacts with diRNA-associated components at DSBs.

In light of this assumption, a yeast two-hybrid assay was performed to screen interactors of *CDC5*, using a small library including RPA2B, RPA1C, RPA1E, RAD51, and *IDN2*, which are localized at DSBs and associated with diRNAs (Liu et al., 2017). Among these components, only *IDN2* interacted with *CDC5* in yeast cells (Figure 3A). The detailed yeast two-hybrid data indicated that the C-terminal region of *IDN2* specifically interacted with the N-terminal region of *CDC5* (Supplemental Figure S8). The further result of in vitro pull-down showed that MBP-tagged *CDC5* was specifically precipitated with the FLAG-tagged *IDN2* (Figure 3B). Moreover, *IDN2*-FLAG was associated with YFP-*CDC5* but not with the free YFP control in plant cells (Figure 3C). Taken together, these results showed that *IDN2* interacts with *CDC5* both in vitro and in vivo, implying their functional association in the DDR.

A previous study reported a role of *IDN2* in HR (Liu et al., 2017), suggesting that the *idn2* mutant might have a defect in DNA repair. According to our real-time PCR results, DNA repair-related genes including *BREAST CANCER SUSCEPTIBILITY1* (*BRCA1*), *POLY (ADP-RIBOSE) POLYMERASE 2* (*PARP2*), and *RAD51* were upregulated in

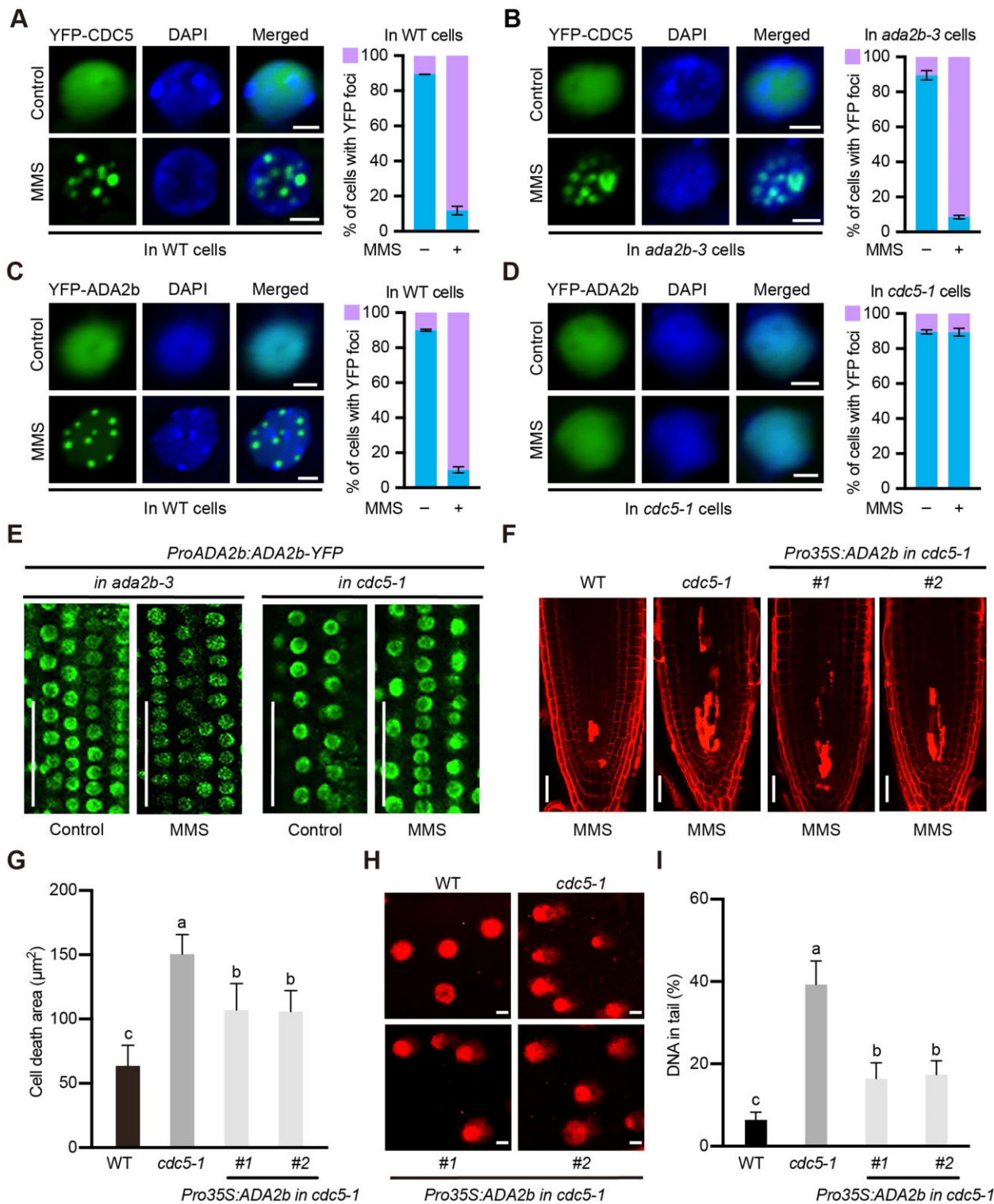


Figure 2 Recruitment of ADA2b at DSBs is mediated by CDC5. A and B, Localization of YFP-CDC5 in wild-type (A) and *ADA2b* mutant (B) protoplasts with and without $100\text{-}\mu\text{g mL}^{-1}$ MMS. C and D, Localization of YFP-ADA2b in wild-type and *CDC5* mutant protoplasts with and without $100\text{-}\mu\text{g mL}^{-1}$ MMS. In the left-hand graphs of (A–D), representative images of YFP (green), DAPI (blue), and merged signals are shown (bars, $2.5\ \mu\text{m}$). In the right-hand graphs of (A–D), percentages of cells with (purple) and without (blue) YFP foci are shown as the mean \pm SD of three independent experiments (independent plant materials and transformation; at least 100 cells were detected in each sample). E, Localization of ADA2b-YFP in roots of *ADA2b* and *CDC5* mutants stably expressing *ADA2b-YFP* driven by its native promoter. Five-day-old seedlings were transferred to medium with or without $100\text{-}\mu\text{g mL}^{-1}$ MMS for 24 h. YFP signals were recorded using confocal microscopy. Bars, $50\ \mu\text{m}$. F and G, Effect of *GFP-ADA2b* overexpression on root cell death induced by DNA damage in the *CDC5* mutant. Five-day-old seedlings were transferred to medium with $100\text{-}\mu\text{g mL}^{-1}$ MMS for 24 h, and then the meristem regions were stained with PI for confocal microscopy. Cell walls and dead cells

(continued)

both *idn2-3* and *cdc5-1* mutant seedlings (Figure 3D). Further comet assay data showed that mutation of *IDN2* led to an accumulation of DNA damage in plants, consistent with mutation of *CDC5* (Figure 3, E and F). Following Zeocin treatment, the survival rates of both *IDN2* and *CDC5* mutants were lower than that of wild-type seedlings (Supplemental Figure S9, A and B). The root development of *idn2-3* was normal under the control condition; however, the cell death level in *idn2-3* roots was significantly higher than that in wild-type roots under treatment with MMS or Zeocin (Figure 3, G and H; Supplemental Figure S9, C and D). These data support the notion that *IDN2* is involved in DNA repair, possibly via a pathway associated with *CDC5*.

Recruitment of *CDC5* at DSBs is dependent on *IDN2*

A previous study showed that *IDN2* is recruited at DSBs, mediating the dissociation of RPA to facilitate the correct localization of *RAD51* (Liu et al., 2017). Moreover, our data indicated that *CDC5* and *ADA2b* form foci at DSBs under DNA damage (Supplemental Figure S4; Lai et al., 2018; Jiang et al., 2019). Consistent with these conclusions, our data showed that *IDN2* was co-localized with both *CDC5* and *ADA2b* at DSB foci (Supplemental Figure S10), supporting the possibility that *IDN2* is involved in the regulation of *SMC5/6* complex.

To further clarify the relationship between *IDN2* and *CDC5* during DSB repair, YFP-*IDN2* was expressed in wild-type and *cdc5-1* protoplasts. Deletion of *CDC5* had no apparent influence on the localization of *IDN2* at DSBs (Figure 4, A and B), as confirmed in stable transgenic lines (Supplemental Figure S11). Conversely, the DSB localization of YFP-*CDC5* under DNA damage was significantly reduced in *idn2-3* mutant cells (Figure 4, C and D). Similarly, YFP-*ADA2b* and *SMC5*-YFP were distributed generally in the nuclei of *idn2-3* cells under MMS treatment (Supplemental Figure S12), supporting the notion that recruitment of the *CDC5*–*ADA2b*–*SMC5* module is dependent on *IDN2*. Then, YFP-*CDC5* driven by its native promoter was introduced into both *idn2-3* and *cdc5-1* mutants to generate stable transgenic plants, in order to confirm the subcellular localization of *CDC5*. The short root phenotype of *cdc5-1* was restored, indicating that the YFP-tagged *CDC5* was functional. The YFP-*CDC5* signal was evenly distributed in the nuclei of transgenic seedlings of both genotypes under the normal condition (Figure 4E). Under MMS treatment, YFP-*CDC5* formed foci in the nuclei of the *CDC5* complementary lines,

but no foci localization of *CDC5* was detectable in the *idn2-3* mutant plants (Figure 4E), consistent with the observations in protoplasts. Therefore, these data from protoplasts and transgenic plants indicate that the recruitment of *CDC5* at DSBs is dependent on *IDN2*.

Given that *CDC5* interacts with *ADA2b* and *IDN2*, it could be supposed that *ADA2b* and *IDN2* would be included in a complex mediated by *CDC5*. To test this hypothesis, the in vivo interaction between *ADA2b* and *IDN2* was detected via a co-immunoprecipitation assay with and without *CDC5* overexpression. The FLAG-tagged *IDN2* was precipitated with the MYC-tagged *ADA2b* in plant cells, and their interaction was enhanced by excess YFP-*CDC5* and MMS treatment, suggesting that *CDC5* functions as a linker in the association of *ADA2b* and *IDN2* (Supplemental Figure S13). In the absence of *IDN2*, trace amounts of *CDC5* at DSBs are not sufficient to enable DNA repair; however, the presence of excess levels of *CDC5* protein may improve its accumulation at DSBs. Therefore, we overexpressed *CDC5* in the *idn2-3* mutant to detect the effect of excess amounts of *CDC5* on the DDR in this background. Cell death was undetectable in seedlings with these genotypes under normal conditions (Supplemental Figure S14). Under the DNA damage condition, areas of dead cells in the roots of *idn2-3* seedlings were significantly attenuated by overexpression of *CDC5* (Figure 4, F and G). The comet assay results showed that overexpression of *CDC5* significantly suppressed DNA fragmentation in the *idn2-3* mutant (Figure 4, H and I). Taken together, this evidence supports the notion that *IDN2* and *CDC5* work together at DSBs to enable DNA repair.

The RNA-binding domain of *IDN2* is crucial for its DSB recruitment

IDN2 is an RNA-binding protein involved in the RNA-directed DNA methylation pathway via its XS domain, which has been predicted to be a double-stranded RNA-binding domain in plants (Ausin et al., 2009; Zhang et al., 2012). Mutation of the XS domain of *IDN2* reduced the HR repair rate in plants (Liu et al., 2017), suggesting that this domain contributes to the function of *IDN2* in DNA repair. Thus, it was important to investigate whether the XS domain is essential for the recruitment of the *CDC5*–*ADA2b*–*SMC5* module at DSBs.

Therefore, following previous reports, a mutant form of *IDN2* (named *IDN2m*) with a point mutation followed by a 24-bp deletion in its XS domain (Ausin et al., 2009) was

Figure 2 (Continued)

were stained by PI (red). Representative images of three biologically independent experiments (independent plant growth and treatment) are shown in (F); bars, 50 μm . Images obtained under normal conditions are shown in Supplemental Figure S7. Cell death areas were calculated using ImageJ, and the quantitative data in (G) are shown as the mean \pm SD from 15 roots. Significant differences are indicated with different letters above the columns; $P < 0.001$, one-way ANOVA followed by Tukey's multiple comparisons test. H and I, Effect of *GFP-ADA2b* overexpression on the DNA integrity of the *CDC5* mutant. The DNA damage status of 3-week-old plants was detected using a comet assay. Representative images from three biologically independent experiments (independent plant growth and sample preparation) are shown in (H); bars, 25 μm . Quantitative data (mean \pm SD) of percentages of DNA in the tail ($n = 15$) are shown in (I). Significant differences are indicated with different letters above the columns; $P < 0.001$, one-way ANOVA followed by Tukey's multiple comparisons test.

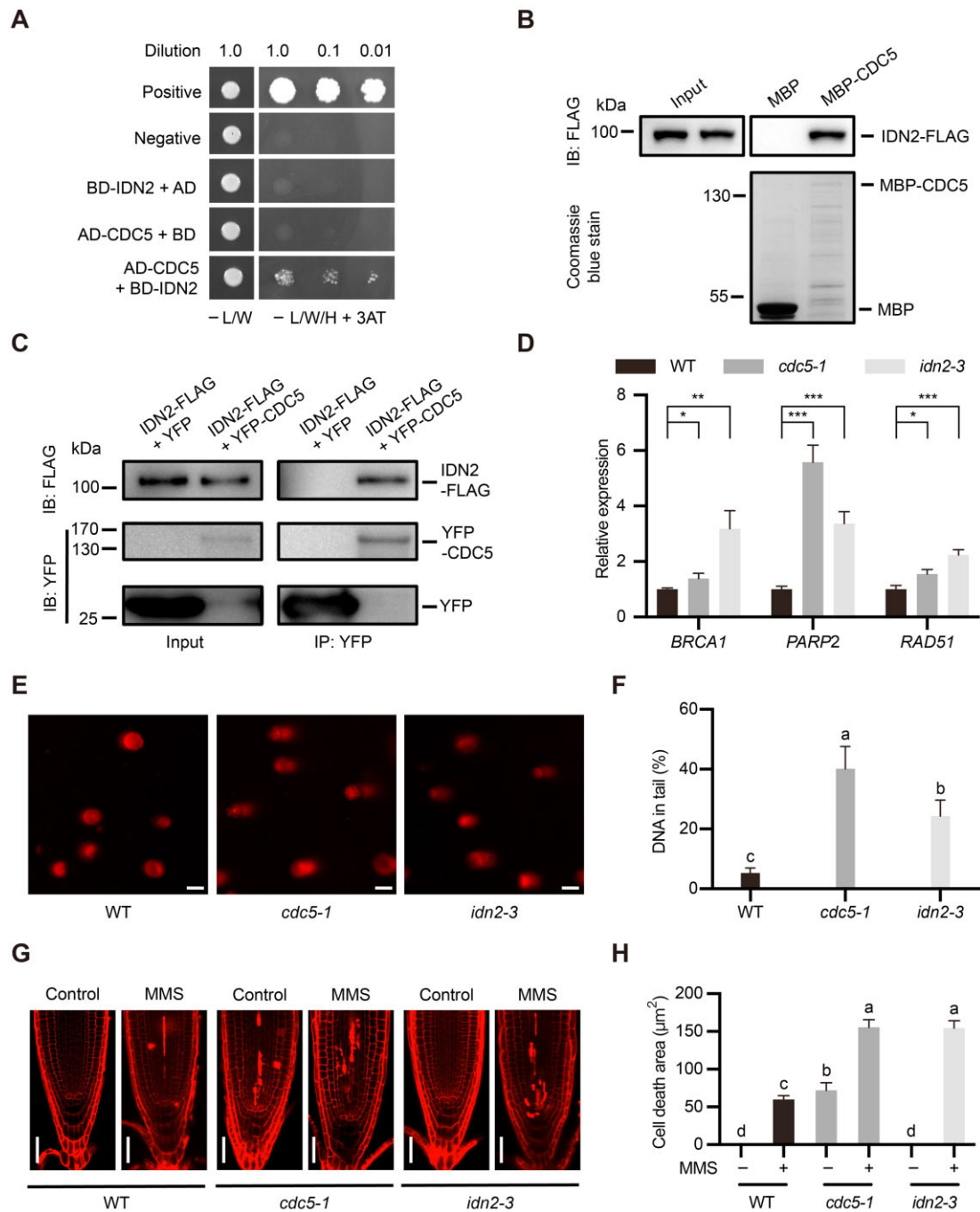


Figure 3 IDN2 interacts with CDC5 and participates in DNA repair. **A**, Yeast two-hybrid assay was used to detect the interaction of IDN2 (fused with BD) and CDC5 (fused with AD). The interaction was determined on SD/-Leu/-Trp/-His medium containing 5-mM 3-AT. **B**, The interaction between IDN2 and CDC5 was detected by an in vitro pull-down assay. CDC5 was fused with an MBP tag, while IDN2 was fused with a FLAG tag. IDN2 precipitated with MBP-CDC5 and free MBP (negative control) were detected with an anti-FLAG antibody. **C**, The association of IDN2 and CDC5 was measured using co-immunoprecipitation in plant cells. IDN2-FLAG was co-expressed with YFP-CDC5 or free YFP (negative control) in protoplasts. Total protein was used for immunoprecipitation (IP) with anti-GFP agarose. The input and IP protein signals were detected via anti-GFP and anti-FLAG antibodies. **D**, Transcript levels of DDR genes in 4-week-old CDC5 and IDN2 mutant plants. The RT-qPCR data are shown as the mean \pm SD from triplicate technical replicates. *** $P < 0.001$, ** $P < 0.01$, * $P < 0.05$, Student's t test (two-tailed). These results are representative of three independent biological experiments (independent plant growth and sample preparation) with similar patterns. **E** and **F**, Detection of DNA damage status in the leaves of 3-week-old CDC5 and IDN2 mutant plants. Representative images from three biologically independent experiments (independent plant growth and sample preparation) are shown in (E); bars, 25 μm . Quantitative data (mean \pm SD) of percentages of DNA in the tail ($n = 20$) are shown in (F). Significant differences are indicated with different letters above the columns; $P < 0.001$, one-way ANOVA followed by Tukey's multiple comparisons test. **G** and **H**, DNA damage sensitivity of the CDC5 and IDN2 mutant seedlings. Five-day-old seedlings were transferred to medium with or without 100- $\mu\text{g mL}^{-1}$ MMS. Twenty-four hours after transfer, cell death in root meristems was detected by PI staining. Representative images from three biologically independent experiments (independent plant growth and treatment) are shown in (G); bars, 50 μm . Cell death areas were calculated using ImageJ, and the quantitative data in (H) are presented as the mean \pm SD from 15 roots. Significant differences are indicated with different letters above the columns; $P < 0.001$, one way ANOVA followed by Tukey's multiple comparisons test.

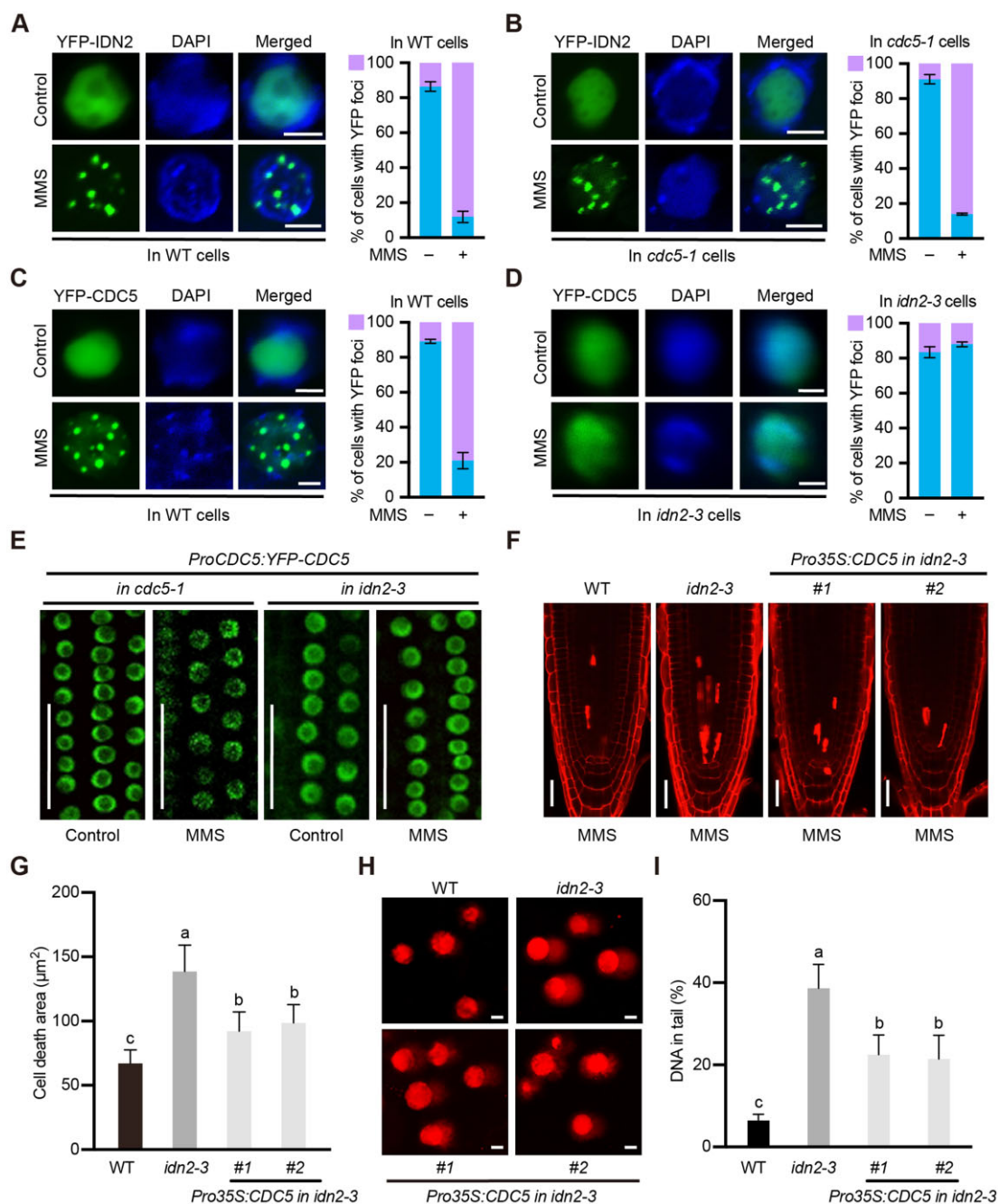


Figure 4 Recruitment of CDC5 at DSBs is dependent on IDN2. A and B, Localization of YFP-IDN2 in wild-type (A) and CDC5 mutant (B) cells with and without 100- $\mu\text{g mL}^{-1}$ MMS. C and D, Localization of YFP-CDC5 in wild-type (C) and IDN2 mutant (D) cells with and without 100- $\mu\text{g mL}^{-1}$ MMS. In the left-hand graphs of (A–D), representative images of YFP (green), DAPI (blue), and merged signals are shown (bars, 2.5 μm). In the right-hand graphs of (A–D), the percentages of cells with (purple) and without (blue) YFP foci are shown as the mean \pm SD from three independent experiments (independent plant materials and transformation; at least 100 cells were detected in each sample). E, Localization of YFP-CDC5 in intact roots of CDC5 and IDN2 mutants transgenically expressing YFP-CDC5. After incubation in medium with or without 100- $\mu\text{g mL}^{-1}$ MMS for 24 h, YFP signals were recorded in 7-day-old seedlings. Representative images are shown in (E); bars, 50 μm . F and G, Effect of YFP-CDC5 overexpression on DNA damage sensitivity of IDN2 mutant roots. After treatment with 100- $\mu\text{g mL}^{-1}$ MMS for 24 h, the root meristems of 7-day-old seedlings were stained with PI, and cell death levels were detected using confocal microscopy. Representative images from three biologically independent experiments (independent plant growth and treatment) are shown in (F); bars, 50 μm . Control images are included in Supplemental Figure S14. Cell death areas were calculated using ImageJ, and quantitative data in (G) are presented as the mean \pm SD from 15 roots. Significant differences are indicated with different letters above the columns; $P < 0.001$, one-way ANOVA followed by Tukey's multiple comparisons test. H and I, DNA integrity of 3-week-old plants was detected by comet assay. Representative images from three biologically independent experiments (independent plant growth and sample preparation) are included in (H); bars, 25 μm . Quantitative data (mean \pm SD) of percentages of DNA in the tail ($n = 15$) are shown in (I). Significant differences are indicated with different letters above the columns; $P < 0.001$, one-way ANOVA followed by Tukey's multiple comparisons test.

fused with YFP for further analyses. Subcellular localization results showed that mutation of the XS domain dramatically attenuated the DSB recruitment of IDN2 in the *idn2-3* mutant background (Figure 5, A and B). This conclusion was confirmed by a localization analysis in stable complementary lines with the YFP-tagged IDN2 or IDN2m (Figure 5C), indicating that the localization of IDN2 at DSBs relied on its dsRNA-binding ability. Co-expression data further indicated that IDN2m failed to recruit CDC5, ADA2b, and SMC5 to DSBs in the *idn2-3* protoplasts (Figure 5, D, E, and F), suggesting that the XS domain of IDN2 is required for the guidance of the SMC5/6 complex to DSBs.

To further confirm the function of the XS domain of IDN2 in the repair of DSBs, complementary plants (Supplemental Figure S15) were subjected to DNA damage treatment. Cell death analysis in root meristem showed that the hypersensitivity of *idn2-3* to MMS was completely inhibited by the wild-type IDN2 but was only slightly suppressed by IDN2m (Figure 5, G and H), providing evidence that the binding of dsRNA is critical for the role of IDN2 during DSB repair.

AGO2 is essential for recruiting the IDN2–CDC5–ADA2b–SMC5/6 module at DSBs

Previous data showed that recruitment of the AGO2/diRNA complex at DSBs provides dsRNA structures for the binding of IDN2 (Liu et al., 2017). Our results indicated that dsRNA binding of IDN2 is essential for recruitment of components of SMC5/6, and previous work has shown that AGO2 binds to diRNAs and is recruited to DSBs via base pairing with nascent transcripts generated from DSBs (Wei et al., 2012; Gao et al., 2014). Therefore, if the DSB recruitment of SMC5/6 is dependent on diRNA, the localization of components including IDN2, CDC5, ADA2b, and SMC5 would be expected to change in the AGO2 mutant.

To test this hypothesis, YFP-IDN2, YFP-CDC5, YFP-ADA2b, and SMC5-YFP were, respectively, expressed in wild-type or *ago2-1* mutant protoplasts with and without MMS treatment. Confocal microscopy results demonstrated that the DSB localization of these components was abolished in the absence of AGO2 (Figure 6, A and B). The DSB recruitment of SMC5-associated components was not altered in *ago3-2*, a mutant of AGO3 that is not related to the diRNA pathway and was used here as a control (Supplemental Figure S16). These data provide evidence for the specific role of the AGO2–diRNA complex in the guidance of the IDN2–CDC5–ADA2b–SMC5/6 module to DSBs.

To characterize the role of AGO2 in DNA repair, we detected the sensitivity of *ago2-1* seedlings to DNA-damaging agents. The *ago2-1* mutants were more sensitive to Zeocin than the wild-type seedlings (Supplemental Figure S17, A and B). Moreover, cell death analysis in root meristems suggested that the 5-day-old *ago2-1* seedlings were more sensitive to both MMS and Zeocin than the wild-type seedlings (Figure 6, C and D; Supplemental Figure S17, C and D). A comet assay using 3-week-old plants indicated

that DNA damage accumulated in the *ago2-1* mutants (Figure 6, E and F). These data suggest that AGO2 plays an important part in plant DNA repair, consistent with our conclusion that the AGO2-mediated diRNA pathway is essential for formation of protein scaffolds for the recruitment of SMC5/6 at DSBs.

Discussion

Accurate recruitment of repair factors at DNA lesions is necessary for the efficiency of DNA repair (Lisby and Rothstein, 2005). The SMC5/6 complex, which maintains chromosome structures in DSB regions, is conserved in eukaryotes (Kegel and Sjögren, 2010; Aragón, 2018). However, the mechanism by which SMC5/6 is precisely targeted to DSBs has remained unclear. Although SLF1/2 in humans and RTT107 in yeasts have been reported to be involved in mediating the DSB localization of SMC5/6 (Leung et al., 2011; Räschele et al., 2015), the original factor that determines the specificity and accuracy of SMC5/6 recruitment is unknown in all species. Based on our previous finding that the transcription co-activator ADA2b is essential for the DSB localization of SMC5/6 in plant cells (Lai et al., 2018), here, we further identified a role for the diRNA-associated IDN2–CDC5–ADA2b protein scaffold in recruitment of SMC5, demonstrating that this protein scaffold is the original determining factor for recruitment of this conserved complex.

Non-coding RNA accumulates at DNA repair foci (Fijen and Rothenberg, 2021), but its function in direct recruitment of the SMC5/6 complex has not previously been reported. DiRNA is generated from DNA regions close to DSBs (Rzeszutek and Betlej, 2020); after binding to AGO2, the diRNA–AGO2 complex targets DSBs, depending on the base pairing between diRNAs and nascent transcripts around the DSB regions (Wei et al., 2012; Gao et al., 2014), to form dsRNA structures for IDN2 recognition (Liu et al., 2017). Our data showed that the dsRNA binding domain is essential for its localization at DSBs and the subsequent CDC5–ADA2b–SMC5 recruitment, supporting the notion that diRNA is necessary for DSB localization of the SMC5/6 complex. This conclusion is further confirmed by our evidence that the DSB localization of all these components, including IDN2, CDC5, ADA2b, and SMC5, is impaired in AGO2 mutant cells. Thus, the diRNA–AGO2 complex precisely recognizes DSBs (Wei et al., 2012), improving the targeting accuracy and specificity of the localization of downstream protein scaffolds for SMC5/6. As diRNA sequences are dependent on the DNA information around DSBs (Yang and Qi, 2015), diRNA originally determines the DSB recruitment of the SMC5/6 complex.

We propose the following model. When DNA damage occurs, diRNAs are generated from the chromatin regions around DSBs. After specifically binding to AGO2, the diRNA–AGO2 complex targets DSBs, together with nascent transcripts, to form dsRNA structures; then, IDN2 binds to dsRNA for its localization at damaged foci. IDN2 interacts with CDC5 and mediates the DSB localization of CDC5,

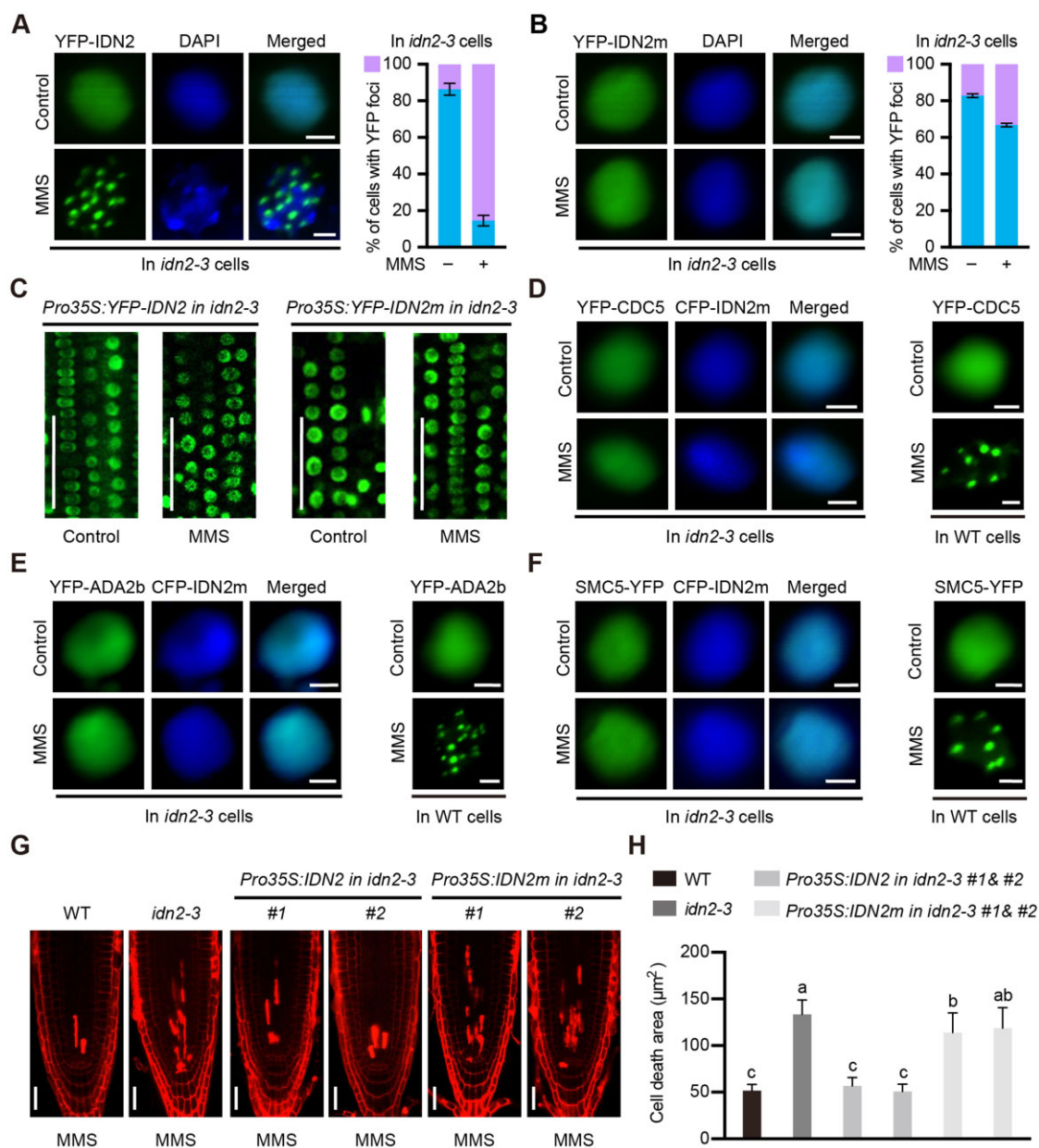
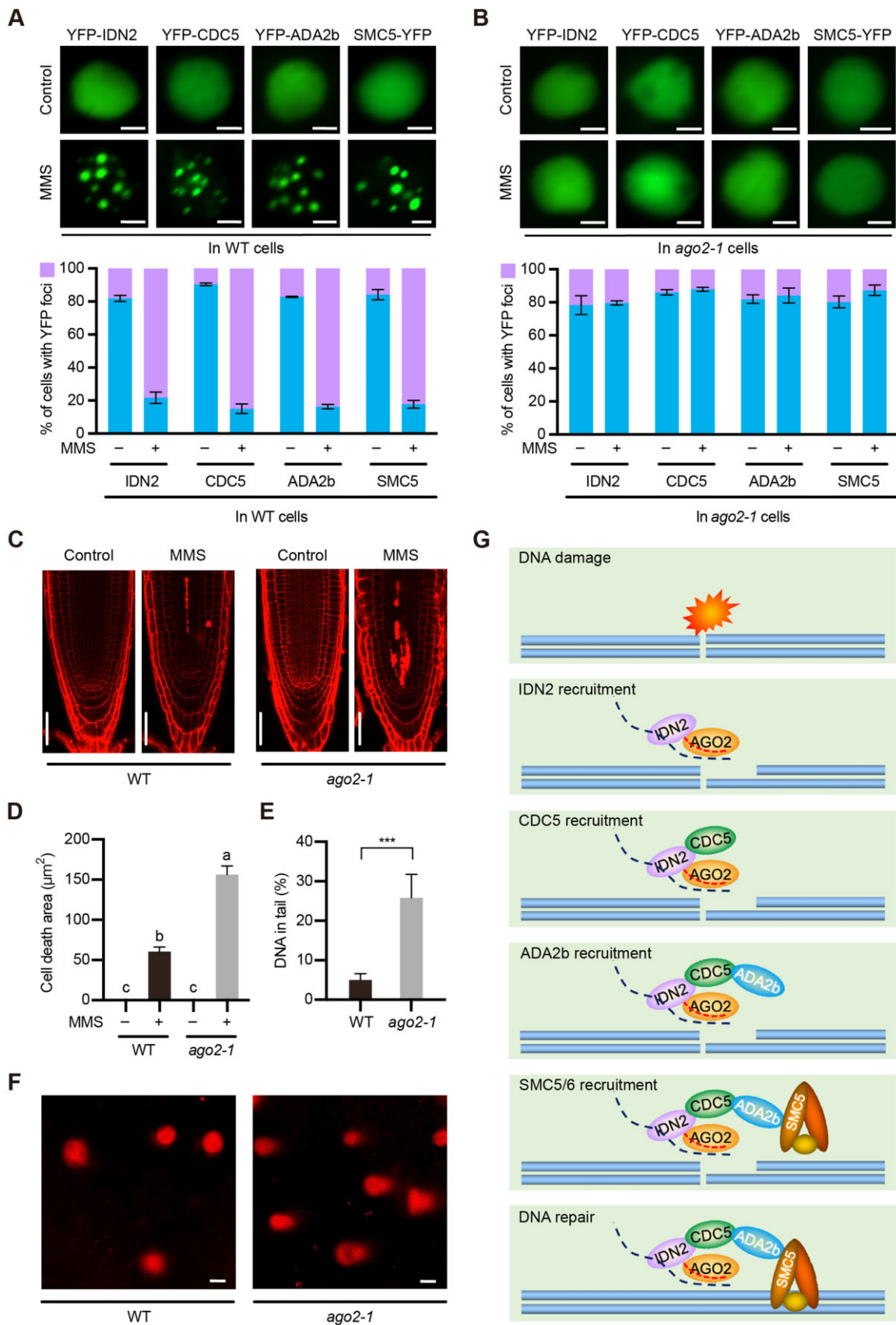


Figure 5 The RNA-binding domain of IDN2 is crucial for its DSB recruitment. A and B, Localization of YFP-IDN2 (A) and YFP-IDN2m (B; mutation in the XS domain for dsRNA binding) in the nuclei of *idn2-3* mutants with and without $100\text{-}\mu\text{g mL}^{-1}$ MMS. In the left-hand graphs of (A, B), representative images of YFP (green), DAPI (blue), and merged signals are shown (bars, $2.5\ \mu\text{m}$). In the right-hand graphs of (A and B), percentages of cells with (purple) and without (blue) YFP foci are shown as the mean \pm SD from three independent experiments (independent plant materials and transformation; at least 100 cells were detected in each sample). C, Localization of YFP-IDN2 and YFP-IDN2m in complementary transgenic plants. The 5-day-old complementary lines were transferred to medium with or without $100\text{-}\mu\text{g mL}^{-1}$ MMS for 24 h. YFP signals in root cells were recorded via confocal microscopy. Bars, $50\ \mu\text{m}$. D–F, Co-localization of IDN2m with CDC5 (D), ADA2b (E), and SMC5 (F) in *idn2-3* mutant protoplasts. CFP-IDN2m was co-expressed with YFP-CDC5, YFP-ADA2b, and SMC5-YFP in *idn2-3* protoplasts treated with or not with $100\text{-}\mu\text{g mL}^{-1}$ MMS for 24 h. Representative images of CFP (green), YFP (blue), and merged signals from three independent experiments (independent plant materials and transformation) are shown. Bars, $2.5\ \mu\text{m}$. G and H, DNA damage sensitivity of roots of IDN2 and IDN2m complementary seedlings. Five-day-old seedlings were treated in medium containing $100\text{-}\mu\text{g mL}^{-1}$ MMS for 24 h before PI staining for cell death analysis. Representative images from three biologically independent experiments (independent plant growth and treatment) are shown in (G); bars, $50\ \mu\text{m}$. Control images are included in Supplemental Figure S15. Cell death areas were calculated using ImageJ, and the quantitative data in (H) are the mean \pm SD from 15 roots. Significant differences are indicated with different letters above the columns; $P < 0.01$, one-way ANOVA followed by Tukey's multiple comparisons test.

while CDC5 associates with ADA2b and determines the DSB recruitment of ADA2b. Given that our previous study showed that ADA2b directly interacts with SMC5 (Lai et al.,

2018), we can conclude that the IDN2–CDC5–ADA2b protein module mediates the DSB recruitment of the SMC5/6 complex for DNA repair (Figure 6G). Because these scaffold



(continued)

proteins belong to distinct large complexes (for instance, CDC5 in MAC and ADA2b in SAGA), it would be interesting to study whether other components in these complexes also contribute to SMC5/6 recruitment. Under normal conditions, because no diRNA is generated, all these components are distributed evenly in the nucleus. Our previous study showed that the SWI/SNF subunit SWI3B enhances dissociation of SMC5 from the chromosome regions where it is originally localized, enabling it to move to DSBs (Jiang et al., 2019). Thus, it will be interesting for further investigations to consider whether all these chromosome-associated scaffold factors need to be detached from their original locations for further DSB targeting.

Additional functions of proteins involved in DNA repair have been reported (Koliadenko and Wilanowski, 2020), suggesting that these factors have multiple roles in DNA repair or other cellular processes. The scaffold proteins identified in SMC5/6 recruitment in this study may have additional functions in DNA repair. For instance, IDN2, which is required for de novo DNA methylation (Ausin et al., 2009), enhances the dissociation of RPA from chromosomes and facilitates the recruitment of RAD51, which also interacts with SMC5/6 for DNA repair (Liu et al., 2017; Chen et al., 2021); CDC5 is a subunit of MAC (Zhang et al., 2013), which plays a part in regulating the cell cycle in the response to DNA damage (Wang et al., 2021); and ADA2b is a partner of the histone acetyltransferase GCN5 (Vlachonasios et al., 2003), which is involved in histone modification around DNA damage sites (Lee et al., 2010). However, the functional connections among these processes are unclear. Therefore, our identification of the IDN2–CDC5–ADA2b scaffold not only contributes to our understanding of the mechanism of SMC5/6 recruitment but also provides insights for further investigation of the associations among these molecular processes during DNA damage. Furthermore, this large complex may also contribute to distinct cellular processes under normal conditions and IP–mass spectra may be used to identify novel components in this complex.

Although the mechanism presented here was obtained using evidence from plant cells, it is worth noting that most of the components identified in this study, including AGO2, CDC5, ADA2b, and SMC5, are conserved proteins in

eukaryotes. Given that IDN2 is a specific protein to plant cells (Ausin et al., 2012), it may be replaced by another component that connects dsRNA and CDC5 in mammalian cells. Therefore, in future studies, it will be important to test our mechanism with respect to whether the association between small RNAs and SMC5/6 is universal among eukaryotes; if this connection also exists in mammalian cells, our work may provide new clues for cancer therapy. Overall, our study identified the original determinant and protein scaffolds for recruitment of the SMC5/6 complex in plant cells, improving our understanding of the precise regulatory mechanism of DNA repair in eukaryotes.

Materials and methods

Plant materials and growth conditions

All seeds used in this work were in the Columbia (*Col-0*) background. The *ada2b-3* (SALK_019407) (Kornet and Scheres, 2009), *cdc5-1* (SAIL_207_F03) (Zhang et al., 2013), *idn2-3* (SALK_152144) (Xie et al., 2012), *ago2-1* (SALK_003380), and *ago3-2* (SALK_005335) (Zhang et al., 2016) seeds were as previously described.

Before being sown on 1/2 Murashige and Skoog (MS) medium with 1.5% (w/v) sucrose and 1% (w/v) agar, the Arabidopsis seeds were surface-sterilized (with 75% [v/v] ethanol for 90 s, then 2.5% [v/v] NaClO solution for 8 min, followed by rinsing 5 times with sterilized water) and stratified at 4°C in the dark for 2 days. The sown seeds were transferred to a greenhouse at 21°C with a light/dark cycle of 16 h/8 h. Light was supplied by white fluorescent tubes (Philips) with an intensity of 80 $\mu\text{E s}^{-1} \text{m}^{-2}$. For MMS or Zeocin treatment, 5-day-old seedlings were transferred to 1/2 MS medium with MMS (Sigma, St Louis, MO, USA, 129925) or Zeocin (Introvigen, Waltham, MA, USA, R25001) for the indicated period before being photographed.

Generation of transgenic plants

Transgenic plants were generated via the floral dip method using *Agrobacterium tumefaciens* strain GV3101 (Clough and Bent, 1998). As the homozygous *ada2b-3* and *cdc5-1* plants are sterile, the constructs were transformed into heterozygous plants of these mutants. Based on genotyping and expression measurement, homozygous transgenic offspring

Figure 6 (Continued)

cells with (purple) and without (blue) YFP foci are presented in the bottom graphs as the mean \pm SD from three biologically independent experiments (independent plant materials and transformation; at least 100 cells were detected in each sample). C, MMS sensitivity of *ago2-1* mutant plants. Five-day-old seedlings were transferred into medium supplemented with or not with 100- $\mu\text{g mL}^{-1}$ MMS for 24 h. Roots were stained with PI, and cell death levels were recorded via confocal microscopy. Representative images from three biologically independent experiments (independent plant growth and treatment) are shown; bars, 50 μm . D, Quantitative data for cell death areas from (C). Cell death areas were calculated using ImageJ, and the data are presented as the mean \pm SD from 15 roots. Significant differences are indicated with different letters above the columns. $P < 0.001$, one-way ANOVA followed by Tukey's multiple comparisons test. E, Quantitative data of percentages of DNA in the tail from (F). Data are presented as the mean \pm SD ($n = 15$). $***P < 0.001$, Student's *t* test (two-tailed). F, Detection of DNA integrity in 3-week-old *ago2-1* leaves via comet assay. Representative images from three biologically independent experiments (independent plant growth and sample preparation) are shown; bars, 25 μm . G, A proposed model for diRNA-dependent recruitment of the SMC5/6 complex during plant DNA damage. The diRNA (a red dashed line) bound to AGO2 targets DSBs together with a nascent transcript (a black dashed line) to form a dsRNA structure for the binding of IDN2. CDC5 functions as a linker between IDN2 and ADA2b, and, finally, ADA2b mediates the recruitment of the SMC5/6 complex at DSBs for DNA repair in plant cells.

plants with a homozygous T-DNA mutant background were used for functional analyses.

For observation of ADA2b in stable transgenic plants, the genomic sequence of *ADA2b* (without the stop codon) with its native promoter was cloned into the *pCAMBIA1300-221-YFP* vector for native expression of *ADA2b-YFP*. To obtain the *ADA2b* overexpression lines, the genomic sequence of *ADA2b* was amplified and cloned into the *pMDC45-GFP* vector to express *GFP-ADA2b* under the control of a 35S promoter. The recombinant plasmid was then transformed into *ada2b-3* and *cdc5-1* heterozygous T-DNA lines.

To obtain lines overexpressing *CDC5* and *IDN2/IDN2m*, the full-length coding regions of *CDC5* and *IDN2/IDN2m* were amplified and cloned into the *pCAMBIA1300-Pro35S:YFP* vector. For native expression of *CDC5* and *IDN2* in stable transgenic plants, their promoter regions were cloned into *pCAMBIA1300-221-YFP*; then, the coding regions of the two genes were cloned into the generated plasmids under the control of their own promoters. The constructs were transformed into the *cdc5-1* heterozygous or *idn2-3* homozygous T-DNA mutant plants.

Yeast two-hybrid assay

The coding sequence (CDS) of *CDC5* was cloned into the *pGADT7* vector and the CDS of *ADA2b* or *IDN2* were cloned into the *pGBKT7* vector, respectively. Yeast two-hybrid experiments were carried out according to the manufacturer's (Clontech) instructions. Interactions were detected on SD/–Leu/–Trp/–His minimal medium supplied with 3-amino-1,2,4-triazole (3-AT). The primers used in this study are given in [Supplemental Data Set 1](#).

Pull-down assay

For detection of the interactions of *CDC5*–*ADA2b* and *CDC5*–*IDN2* in vitro, the CDS of *CDC5* was cloned into *pMAL-c2X* fused with a MBP tag, and the CDS of *ADA2b* or *IDN2* was cloned into *pCDFDuet-1* with a FLAG tag. These constructs were transformed into the *Escherichia coli* BL21 strain. Colonies were amplified and incubated with 0.5-mM IPTG overnight for protein expression. The bacteria were then collected and total protein was extracted with binding buffer (50-mM Tris–HCl pH 7.4, 120-mM NaCl, 5% [v/v] glycerol, 0.5% [v/v] Nonidet P-40, 1 mM PMSF, and 1-mM β -mercaptoethanol). The MBP-*CDC5* and empty MBP (negative control) extracts were incubated with amylose resin (Sangon Biotech, Shanghai, China, C500096) for 60 min at room temperature. The resins were then collected for incubation with the *ADA2b*-FLAG or *IDN2*-FLAG extract for 60 min at room temperature. After being rinsed 5 times with washing buffer (50-mM Tris–HCl pH 7.4, 120-mM NaCl, 5% [v/v] glycerol, and 0.5% [v/v] Nonidet P-40), all the samples were mixed with protein sample buffer, boiled for 3 min and subjected to sodium dodecyl sulfate–polyacrylamide gel electrophoresis (SDS/PAGE). Then, the protein samples were transferred to polyvinylidene fluoride membranes via a BIO-RAD Trans-BlotTurbo system and immunoblotted using anti-FLAG antibody (TransGen, HT201-01, at a

1:10,000 dilution) and anti-mouse IgG (CST, #7076, at a 1:10,000 dilution).

Co-immunoprecipitation

Co-immunoprecipitation was performed to detect the interactions of *CDC5*–*ADA2b* and *CDC5*–*IDN2* in vivo. *ADA2b* or *CDC5* was cloned into a *pBluescript*-based *Pro35S:YFP* vector for expression of YFP-*ADA2b* or YFP-*CDC5*. *CDC5* or *IDN2* was fused with a FLAG tag and cloned into a *pBluescript*-based vector under the control of a 35S promoter. In protoplasts, *Pro35S:YFP-ADA2b* or *Pro35S:YFP* (negative control) was co-transformed with *Pro35S:CDC5-FLAG*; or *Pro35S:YFP-CDC5* or *Pro35S:YFP* (negative control) was co-transformed with *Pro35S:IDN2-FLAG*. After transformation, the protoplasts were incubated for 48 h before harvest. The collected cells were then incubated with extraction buffer (10-mM Tris–HCl pH 7.4, 100-mM NaCl, 10% [v/v] glycerol, 0.5% [v/v] Nonidet P-40) with protease inhibitor cocktail (Roche, Basel, Switzerland). Then, the extracts were centrifuged at 13,000 g at 4°C for 15 min, and the supernatants were incubated with **GFP-Trap resin (AlpaLife, KTSM1301) at 4°C for 3 h**. The GFP-Trap resin was collected and rinsed with washing buffer (10-mM Tris–HCl pH 7.4, 100-mM NaCl, 10% [v/v] glycerol) 3 times. All samples were mixed with protein sample buffer and boiled for 3 min before analysis via SDS/PAGE and immunoblotting with anti-FLAG antibody (TransGen, HT201-01, at a 1:10,000 dilution) or anti-GFP (TransGen, HT801-01, at a 1:10,000 dilution), and anti-mouse IgG (CST, #7076, at a 1:10,000 dilution).

To detect the interaction between *ADA2b* and *IDN2* in vivo, *ADA2b* was fused with 5 \times MYC and cloned into the *pBluescript*-based vector under the control of a 35S promoter. *Pro35S:MYC-ADA2b* was co-transformed with *Pro35S:IDN2-FLAG* with or without *Pro35S:YFP-CDC5* in protoplasts (*Pro35S:MYC* vector was used in the negative control). Co-immunoprecipitation was conducted as described above using **anti-MYC Nanobody Agarose Beads (AlpaLife, KTSM1306)**. The samples were analyzed via SDS/PAGE and immunoblotted with anti-FLAG antibody (TransGen, HT201-01, at a 1:10,000 dilution), anti-GFP antibody (TransGen, HT801-01, at a 1:10,000 dilution), and anti-MYC antibody (TransGen, HT101-01, at a 1:10,000 dilution).

Gene expression analysis

RNA was extracted from the rosette leaves of plants with different genotypes using a HiPure Plant RNA Mini Kit (Magen, R4151-02) following the manufacturer's instructions. HiScript III 1st Strand cDNA Synthesis Kit with Oligo(dT) (Vazyme, Nanjing, China, R312-01/02) was used for reverse transcription. RT-qPCR was performed using a Bio-Rad CFX 96 system (C1000 Thermal Cycler) and the expression levels were analyzed using the $2^{-\Delta\Delta C_q}$ method by Bio-Rad CFX Manager software version 2.1.

Comet assay

Comet assays were performed using protoplasts from 3-week-old plants, according to the instructions of the Comet

Assay Kit (Trevigen, Gaithersburg, MD, USA, 4250-050-K). Slides were stained with SYBR Gold (Life Technologies, Carlsbad, CA, USA) and observed under a confocal microscope (Zeiss LSM 710 or 800 confocal microscope) with excitation and emission wavelengths of 488 and 505–530 nm, respectively. The degree of DNA damage was analyzed with CASP Comet Assay Software.

Fluorescence microscopy

To determine the localization of the target proteins in protoplasts, the CDS of *CDC5* and *IDN2* were cloned into *Pro35S:CFP/YFP* based on a *pBluescript* vector. The plasmids *YFP-ADA2b* and *SMC5-YFP* were as described in our previous report (Lai et al., 2018). The constructs were transformed into the indicated protoplasts and incubated with or without MMS (Sigma, 129925) in W5 solution (Yoo et al., 2007). DAPI (Sigma, D9542) was used for nuclear staining.

For the observation of roots, 5-day-old transgenic seedlings were transferred into 1/2 MS medium with or without MMS/Zeocin as described in the figure legends; 10- $\mu\text{g mL}^{-1}$ PI (Sangon Biotech, A601112) was used for cell wall staining in roots before observation. Signals were detected with a Zeiss LSM 800 confocal microscope.

Statistical analysis

Student's *t* test (two-tailed) was used to evaluate significant differences between wild-type and the indicated mutants. One-way ANALYSIS OF VARIANCE (ANOVA) followed by Tukey's multiple comparisons test was used to compare the differences between each genotype, and significant differences are indicated with different letters above the columns. Statistical analyses were performed using Prism 8 software. The *t* test and ANOVA results are shown in Supplemental Data Set 2.

Accession numbers

The sequences used in this work were obtained from the Arabidopsis Genome Initiative (<https://www.arabidopsis.org/>) with the following accession numbers: *ADA2b* (AT4G16420), *SMC5* (AT5G15920), *CDC5* (AT1G09770), *IDN2* (AT3G48670), *AGO2* (AT1G31280), *BRCA1* (AT4G21070), *RAD51* (AT5G20850), *PARP2* (AT4G02390), and *ACTIN2* (AT3G18780).

Supplemental data

The following materials are available in the online version of this article.

Supplemental Figure S1. The domains involved in the interaction between *CDC5* and *ADA2b*.

Supplemental Figure S2. Detection of DNA damage in the *ADA2b* or *CDC5* complementary plants.

Supplemental Figure S3. The sensitivity of the *ADA2b* and *CDC5* mutants to Zeocin.

Supplemental Figure S4. Co-localization of *CDC5* with *ADA2b* and *SMC5* in protoplasts.

Supplemental Figure S5. Localization of *SMC5* in the wild-type and *cdc5-1* mutant protoplasts.

Supplemental Figure S6. Localization of *YFP-CDC5* in intact roots of the *CDC5* or *ADA2b* mutant transgenically expressing *YFP-CDC5*.

Supplemental Figure S7. Detection of the effect of *ADA2b* overexpression on cell death in root meristems of *cdc5-1* without MMS treatment.

Supplemental Figure S8. The domains involved in the interaction between *CDC5* and *IDN2*.

Supplemental Figure S9. The sensitivity of the *cdc5-1* and *idn2-3* mutants to Zeocin.

Supplemental Figure S10. Co-localization of *IDN2* with *CDC5* and *ADA2b* in protoplasts.

Supplemental Figure S11. Localization of *YFP-IDN2* in *idn2-3* or *cdc5-1* mutant seedlings transgenically expressing *YFP-IDN2*.

Supplemental Figure S12. Localization of *ADA2b* and *SMC5* in the wild-type and *idn2-3* mutant protoplasts.

Supplemental Figure S13. Detection of in vivo interaction between *ADA2b* and *IDN2* with or without *CDC5* overexpression.

Supplemental Figure S14. Detection of the effect of *CDC5* overexpression on cell death in root meristems of *idn2-3* without MMS treatment.

Supplemental Figure S15. Detection of cell death in root meristems of the *IDN2* and *IDN2m* complementary plants without MMS treatment.

Supplemental Figure S16. Localization of *IDN2* and *SMC5* in the wild-type and *ago3-2* mutant protoplasts.

Supplemental Figure S17. The sensitivity of the *ago2-1* mutant to Zeocin.

Supplemental Data Set 1. Primers used in this study.

Supplemental Data Set 2. The *t* test and ANOVA results in this study.

Acknowledgments

We thank the Arabidopsis Biological Resource Center for the mutant seeds used in this study. We also thank Professor Yijun Qi (Tsinghua University) for the *idn2-3* mutant seeds.

Funding

This work was supported by the Major Program of Guangdong Basic and Applied Research (2019B030302006), the National Natural Science Foundation of China (31871222, 31970531, 31771504, 32000493, and 31771349), the National Science Foundation of Guangdong (2018B030308002, 2020A1515010964, and 2021A1515011151), Guangdong Modern Agro-industry Technology Research System (2021KJ114), China Postdoctoral Science Foundation (2018M643111), the Program for Changjiang Scholars, the Guangdong Special Support Program of Young Top-Notch Talent in Science and Technology Innovation (2019TQ05N651), and Pearl River Talent Plan (2019QN01N108).

Conflict of interest statement. None declared.

References

- Aragón L** (2018) The Smc5/6 complex: new and old functions of the enigmatic long-distance relative. *Annu Rev Genet* **52**: 89–107
- Ausin I, Greenberg MVC, Simanshu DK, Hale CJ, Vashisht AA, Simon SA, Lee T, Feng S, Española SD, Meyers BC, et al.** (2012) Involved in De Novo 2-containing complex involved in RNA-directed DNA methylation in Arabidopsis. *Proc Natl Acad Sci USA* **109**: 8374–8381
- Ausin I, Mockler TC, Chory J, Jacobsen SE** (2009) IDN1 and IDN2 are required for De Novo DNA methylation in *Arabidopsis thaliana*. *Nat Struct Mol Biol* **16**: 1325–1327
- Ceccaldi R, Rondinelli B, D’Andrea AD** (2016) Repair pathway choices and consequences at the double-strand break. *Trends Cell Biol* **26**: 52–64
- Chankova SG, Dimova E, Dimitrova M, Bryant PE** (2007) Induction of DNA double-strand breaks by zeocin in *Chlamydomonas reinhardtii* and the role of increased DNA double-strand breaks rejoining in the formation of an adaptive response. *Radiat Environ Biophys* **46**: 409–416
- Chen H, He C, Wang C, Wang X, Ruan F, Yan J, Yin P, Wang Y, Yan S** (2021) RAD51 supports DMC1 by inhibiting the SMC5/6 complex during meiosis. *Plant Cell* **33**: 2869–2882
- Clough SJ, Bent AF** (1998) Floral dip: a simplified method for Agrobacterium-mediated transformation of *Arabidopsis thaliana*. *Plant J* **16**: 735–743
- Diaz M, Pecinka A** (2018) Scaffolding for repair: understanding molecular functions of the SMC5/6 complex. *Genes (Basel)* **9**: 36
- Fijen C, Rothenberg E** (2021) The evolving complexity of DNA damage foci: RNA, condensates and chromatin in DNA double-strand break repair. *DNA Repair (Amst)* **105**: 103170
- Friedberg EC, McDaniel LD, Schultz RA** (2004) The role of endogenous and exogenous DNA damage and mutagenesis. *Curr Opin Genet Dev* **14**: 5–10
- Gao M, Wei W, Li MM, Wu YS, Ba Z, Jin KX, Li MM, Liao YQ, Adhikari S, Chong Z, Zhang T, et al.** (2014) Ago2 facilitates Rad51 recruitment and DNA double-strand break repair by homologous recombination. *Cell Res* **24**: 532–541
- Gobbini E, Cesena D, Galbiati A, Lockhart A, Longhese MP** (2013) Interplays between ATM/Tel1 and ATR/Mec1 in sensing and signaling DNA double-strand breaks. *DNA Repair (Amst)* **12**: 791–799
- Harvey SH, Sheedy DM, Cuddihy AR, O’Connell MJ** (2004) Coordination of DNA damage responses via the Smc5/Smc6 complex. *Mol Cell Biol* **24**: 662–674
- Hu Z, Cools T, De Veylder L** (2016) Mechanisms used by plants to cope with DNA damage. *Annu Rev Plant Biol* **67**: 439–462
- Jackson SP, Bartek J** (2009) The DNA-damage response in human biology and disease. *Nature* **461**: 1071–1078
- Jeppsson K, Kanno T, Shirahige K, Sjögren C** (2014) The maintenance of chromosome structure: positioning and functioning of SMC complexes. *Nat Rev Mol Cell Biol* **15**: 601–614
- Jiang J, Mao N, Hu H, Tang J, Han D, Liu S, Wu Q, Liu Y, Peng C, Lai J, et al.** (2019) A SWI/SNF subunit regulates chromosomal dissociation of structural maintenance complex 5 during DNA repair in plant cells. *Proc Natl Acad Sci USA* **116**: 15288–15296
- Kegel A, Sjögren C** (2010) The SMC5/6 complex: more than repair? *Cold Spring Harb Symp Quant Biol* **75**: 179–187
- Kinner A, Wu W, Staudt C, Iliakis G** (2008) Gamma-H2AX in recognition and signaling of DNA double-strand breaks in the context of chromatin. *Nucleic Acids Res* **36**: 5678–5694
- Koliadenko V, Wilanowski T** (2020) Additional functions of selected proteins involved in DNA repair. *Free Radic Biol Med* **146**: 1–15
- Kornet N, Scheres B** (2009) Members of the GCN5 histone acetyltransferase complex regulate PLETHORA-mediated root stem cell niche maintenance and transit amplifying cell proliferation in Arabidopsis. *Plant Cell* **21**: 1070–1079
- Kowalczykowski SC** (2015) An overview of the molecular mechanisms of recombinational DNA repair. *Cold Spring Harb Perspect Biol* **7**: 1–36
- Lai J, Jiang J, Wu Q, Mao N, Han D, Hu H, Yang C** (2018) The transcriptional coactivator ADA2b recruits a structural maintenance protein to double-strand breaks during DNA repair in plants. *Plant Physiol* **176**: 2613–2622
- Lee HS, Park JH, Kim SJ, Kwon SJ, Kwon J** (2010) A cooperative activation loop among SWI/SNF, γ -H2AX and H3 acetylation for DNA double-strand break repair. *EMBO J* **29**: 1434–1445
- Leung GP, Lee L, Schmidt TI, Shirahige K, Kobor MS** (2011) Rtt107 is required for recruitment of the SMC5/6 complex to DNA double strand breaks. *J Biol Chem* **286**: 26250–26257
- Lieber MR** (2010) The mechanism of double-strand DNA break repair by the Nonhomologous DNA end-joining pathway. *Annu Rev Biochem* **79**: 181–211
- Lin Z, Yin K, Zhu D, Chen Z, Gu H, Qu LJ** (2007) AtCDC5 regulates the G2 to M transition of the cell cycle and is critical for the function of Arabidopsis shoot apical meristem. *Cell Res* **17**: 815–828
- Lisby M, Rothstein R** (2005) Localization of checkpoint and repair proteins in eukaryotes. *Biochimie* **87**: 579–589
- Liu M, Ba Z, Costa-Nunes P, Wei W, Li L, Kong F, Li Y, Chai J, Pontes O, Qi Y** (2017) IDN2 interacts with RPA and facilitates DNA double-strand break repair by homologous recombination in Arabidopsis. *Plant Cell* **29**: 589–599
- Murray JM, Carr AM** (2008) Smc5/6: a link between DNA repair and unidirectional replication? *Nat Rev Mol Cell Biol* **9**: 177–182
- Potts PR, Porteus MH, Yu H** (2006) Human SMC5/6 complex promotes sister chromatid homologous recombination by recruiting the SMC1/3 cohesin complex to double-strand breaks. *EMBO J* **25**: 3377–3388
- Puchta H** (2005) The repair of double-strand breaks in plants: mechanisms and consequences for genome evolution. *J Exp Bot* **56**: 1–14
- Räschle M, Smeenk G, Hansen RK, Temu T, Oka Y, Hein MY, Nagaraj N, Long DT, Walter JC, Hofmann K, et al.** (2015) Proteomics reveals dynamic assembly of Repair complexes during bypass of DNA cross-links. *Science* **348**: 1253671
- Rzeszutek I, Betlej G** (2020) The role of small noncoding RNA in DNA double-strand break repair. *Int J Mol Sci* **21**: 1–13
- Schubert I** (2021) Boon and bane of DNA double-strand breaks. *Int J Mol Sci* **22**: 5171
- Storici F, Tichon AE** (2017) RNA takes over control of DNA break repair. *Nat Cell Biol* **19**: 1382–1384
- Su TT** (2006) Cellular responses to DNA damage: one signal, multiple choices. *Annu Rev Genet* **40**: 187–208
- Syed A, Tainer JA** (2018) The MRE11-RAD50-NBS1 complex conducts the orchestration of damage signaling and outcomes to stress in DNA replication and repair. *Annu Rev Biochem* **87**: 263–294
- Turinetto V, Giachino C** (2015) Survey and summary multiple facets of histone variant H2AX: a DNA double-strand-break marker with several biological functions. *Nucleic Acids Res* **43**: 2489–2498
- Vlachonasis KE, Thomashow MF, Triezenberg SJ** (2003) Disruption mutations of ADA2b and GCN5 transcriptional adaptor genes dramatically affect Arabidopsis growth, development, and gene expression. *Plant Cell* **15**: 626–638
- Wang L, Zhan L, Zhao Y, Huang Y, Wu C, Pan T, Qin Q** (2021) The ATR-WEE1 kinase module inhibits the MAC complex to regulate alternative splicing during replication stress. *Nucleic Acids Res* **3**: 1–34
- Watanabe K, Pacher M, Dukowic S, Schubert V, Puchta H, Schubert I** (2009) The STRUCTURAL MAINTENANCE OF CHROMOSOMES 5/6 complex promotes sister chromatid

- alignment and homologous recombination after DNA damage in *Arabidopsis thaliana*. *Plant Cell* **21**: 2688–2699
- Waterman DP, Haber JE, Smolka MB** (2020) Checkpoint responses to DNA double-strand breaks. *Annu Rev Biochem* **89**: 103–133
- Wei W, Ba Z, Gao M, Wu Y, Ma Y, Amiard S, White CI, Danielsen JMR, Yang YG, Qi Y** (2012) A role for small RNAs in DNA double-strand break repair. *Cell* **149**: 101–112
- Xie M, Ren G, Costa-Nunes P, Pontes O, Yu B** (2012) A subgroup of SGS3-like proteins act redundantly in RNA-directed DNA methylation. *Nucleic Acids Res* **40**: 4422–4431
- Yang YG, Qi Y** (2015) RNA-directed repair of DNA double-strand breaks. *DNA Repair (Amst)* **32**: 82–85
- Yatskevich S, Rhodes J, Nasmyth K** (2019) Organization of chromosomal DNA by SMC complexes. *Annu Rev Genet* **53**: 445–482
- Yoo SD, Cho YH, Sheen J** (2007) *Arabidopsis* mesophyll protoplasts: a versatile cell system for transient gene expression analysis. *Nat Protoc* **2**: 1565–1572
- Zhang CJ, Ning YQ, Zhang SW, Chen Q, Shao CR, Guo YW, Zhou JX, Li L, Chen S, He XJ** (2012) IDN2 and its paralogs form a complex required for RNA-directed DNA methylation. *PLoS Genet* **8**: e1002693
- Zhang S, Xie M, Ren G, Yu B** (2013) CDC5, a DNA binding protein, positively regulates posttranscriptional processing and/or transcription of primary microRNA transcripts. *Proc Natl Acad Sci USA* **110**: 17588–17593
- Zhang Z, Liu X, Guo X, Wang XJ, Zhang X** (2016) *Arabidopsis* AGO3 predominantly recruits 24-nt small RNAs to regulate epigenetic silencing. *Nat Plants* **2**: 1–7